2020 IEEE International Conference on Robotics and Automation (ICRA)
31 May - 31 August, 2020. Paris, France

Passive Dynamic Balancing and Walking in Actuated Environments

Jenna Reher[1*], Noel Csomay-Shanklin[1*], David L. Christensen[2], Bobby Bristow[2], Aaron D. Ames[1], and Lanny Smoot[2]

***Abstract*— The control of passive dynamic systems remains a challenging problem in the field of robotics, and insights from their study can inform everything from dynamic behaviors on actuated robots to robotic assistive devices. In this work, we explore the use of flat actuated environments for realizing passive dynamic balancing and locomotion. Specifically, we utilize a novel omnidirectional actuated floor to dynamically stabilize two robotic systems. We begin with an inverted pendulum to demonstrate the ability to control a passive system through an active environment. We then consider a passive bipedal robot wherein dynamically stable periodic walking gaits are generated through an optimization that leverages the actuated floor. The end result is the ability to demonstrate passive dynamic walking experimentally through the use of actuated environments.**

I. Introduction

The study of passive dynamic walking has a long and rich history dating back to the seminal work of McGeer [1]. It was discovered that passive robots walking down shallow slopes—wherein the slope and gravity provide the energy to power the system, i.e., the world actuates the robot—can walk dynamically in a stable fashion [2]. The properties of these systems have since been studied in great detail, including their stability [2], [3], the ability to use minimal actuation to achieve walking [4], [5], [6], [7], and embedding passive walking to achieve 3D locomotion [8], [9]. Similar ideas relating to simple representations of dynamic walking also lead to the foundational work of Raibert on quadrupeds [10]. Importantly, the understanding gained on dynamic walking through the study of the natural nonlinear passive dynamics of these robots has had impact on a variety of applications: from dynamic walking on actuated robots [11], [12], [13], [14], [15] to robotic assistive devices [16], [17].

The primary goal of this work is to take the study of passive dynamic locomotion into a new direction through studying the stabilization of dynamic robotic systems in *actuated environments*. While the excitation of passive motions through actuated environments has been studied in other works [18], to the authors' knowledge this has not been applied to hybrid or legged platforms. This can be seen as philosophically building on the work of passive dynamic walking, where now the world can actuate the system rather than through the passive coupling between potential and kinetic energy provided by walking down a slope. The study of the role of actuated environments in this work is made possible through a novel actuated floor [19], [20], [21] that provides a new paradigm for omnidirectional treadmills. We utilize this actuated floor to study the stability of two robotic systems: an inverted pendulum and passive walker.

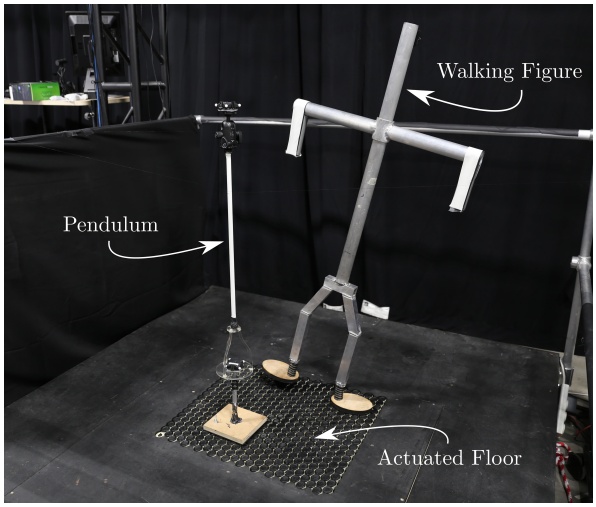

Fig. 1. The pendulum and passive walker atop an actuated floor.

Inverted pendulum models have been extensively studied in the fields of nonlinear dynamics and control [22], [23], [24], [25]. Due to their relatively simple nonlinear dynamics, the balancing of inherently unstable inverted pendulums has served as a benchmark for testing controllers [26]. Additionally, inverted pendulums play a central role in understanding control and gait generation for bipedal robots [27], [28], [29], [30]. The first result of this paper is the stabilization of a passive inverted pendulum — both upright and with tracking of desired trajectories at its base — which serves to demonstrate the active floor control paradigm experimentally.

The main result of this paper is the realization of passive dynamic walking through the use of an actuated floor using a simple robot armature and an omnidirectional treadmill shown in Fig. 1. To achieve this result, we begin with a hybrid system model of the robot as it interacts with the floor—this encodes the nonlinear continuous dynamics and discrete transitions that occur at foot strike. A stable periodic orbit is generated for this hybrid model through the use of nonlinear optimization. This is realized experimentally through control of the actuated floor, with the result being a dynamically stable walking gait. This provides the first example of passive dynamic walking with actuated environments.

*These authors contributed equally to this work, and were employees of Disney Research during the time of this project.

[1]J. Reher, N. Csomay-Shanklin, and A. Ames are with the Departments of Mechanical and Civil Engineering and Computing and Mathematical Sciences, California Institute of Technology, Pasadena, CA 91125 USA. {jreher, noelcs, ames}@caltech.edu

[2]D. Christensen, B. Bristow, and L. Smoot are with Disney Research, 521 Circle Seven Drive, Glendale, CA 91201, USA. {david.l.christensen, bobby.bristow, lanny.s.smoot}@disney.com

978-1-7281-7395-5/20/$31.00 ©2020 IEEE

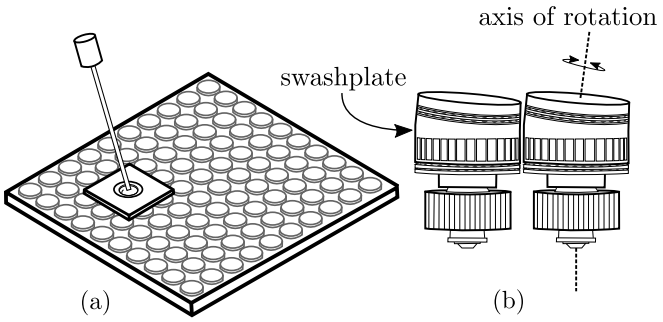

Fig. 2. Depiction of the omnidirectional platform showing: (a) the tiled floor with a grid of actuated disks and (b) side profile of the disks, showing the angled tilt controlled by rotating a swashplate and the top disk which is separately actuated to drive linear velocities on the floor.

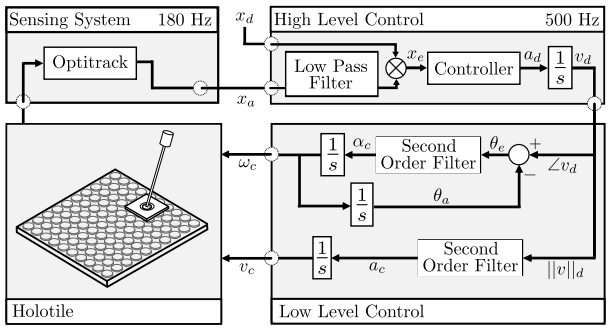

Fig. 3. Hardware architecture for the actuated platform. Two computers provide the sensing and high level control of the floor, respectively, while an Arduino translates the high level commands into a signal for the stepper-motors in the floor.

The paper is structured as follows: Section II introduces the omnidirectionally actuated platform and associated sensing, estimation, and low-level infrastructure which is used in this work. Section III describes several controllers which can be used on the platform for stabilizing inverted pendulums and demonstrates their performance on an actuated floor experimentally. Section IV introduces a passive dynamic bipedal structure which can be dynamically animated into a limit cycle while balancing on the floor. Lastly, Section V discusses the conclusions and future work.

II. THE ACTUATED ENVIRONMENT

In this paper, the actuation from the environment is provided by a novel omnidirectional platform developed by Disney Research [19], [20], [21]. The platform is a floor which consists of an array of tilted motor-driven disks supported by swashplates, and is depicted in Fig. 2. Because the disk heads are tilted, all actuation is transmitted through friction with any objects resting on the floor that are touching the raised curvature of the disk. The swashplate is sandwiched between two bearings to decouple the rotation of two motors driving the disk and tilt orientation, respectively. The rotation of the swashplate points the upper disk edges to control the direction of movement of objects on its surface, while the rotational velocity of the disk itself determines the linear speed of an object on the surface.

The floor surface was designed to support high walking speeds (up to 2 meters second) and high accelerations (up to 2 G) while supporting over 100 kg loads and providing rapid directional change capabilities. The authors felt that these characteristics would also lend the omnidirectional control surface to balancing problems that could ultimately lead to passive or minimally actuated robots that were not necessarily capable of independent locomotion or balancing to be stabilized on the floor. The treadmill movable area is 0.66 m by 0.5 m surrounded by a 1.5 m square platform to provide a flat surface when stepping off of the actuated tiles.

A. Sensing

In order to provide the appropriate control across a variety of applications, the sensing of accurate position, rotation, and Cartesian velocities for the object being balanced is desired. Six Optitrack Prime 13 cameras were mounted at the top of an overhead platform and directed towards the omnidirectional floor to ensure that markers on the object to be balanced were always visible to a minimum of three cameras. A standalone PC was used to collect the camera stream, which is then connected via UDP to a computer dedicated to computing the desired control input for the floor.

The Optitrack sensing system provides very accurate positions and rotations of the active pucks, but does not provide velocities. As such, we apply a lowpass filter to the positional data and numerically differentiate the filtered position to obtain a smooth velocity profile.

B. Control Interface

The high level controllers receive the state information and provide a desired acceleration vector based on the difference between the actual and desired states. However, because the floor is driven by two stepper motors, this must be converted into a velocity profile which can be sent as step commands. To handle this, we integrate the acceleration commands received at the high level and apply the resulting velocity. However, in some situations this caused windup similar to integral windup in traditional PID controllers. To make the controller more responsive, we used a leaky integrator:

$$v_{\mathrm{cmd},k} = C \cdot v_{\mathrm{cmd},k-1} + a_{cmd,k} dt, \tag{1}$$

where C is a tuneable constant for the rate of 'leak'. For the work presented here, C was typically tuned between the values of 0.990 and 0.998. The specifics of the various controllers applied are discussed in the next section, with the resulting command sent over serial to our low level controller running on an Arduino Mega. At this level, various filtering and feedback is performed so as not to exceed the hardware limitations of the system, such as maximum torque and speed. The combination of sensing, and high and low level controllers can be seen in Figure 3. Note that the direction-changing bandwidth of the platform is limited by the maximum rotational speed of the swashplates when motions different from the current direction are required. This occurs because limited cog-rate stepper motors drive these plates and software limits prevent over-speed.

III. Inverted Pendulum on an Actuated Floor

In this section we investigate several control methods for stabilizing and target tracking of a inverted pendulum. This will be built on in Section IV when it is applied to balance one plane of a passive dynamic walker.

A. Inverted Pendulum Modeling

First, we consider the dynamics and control of an inverted pendulum which is placed on the treadmill surface. We can define coordinates for the system as $q := (x_b, y_b, \delta_x, \delta_y) \in \mathcal{Q} \subseteq \mathbb{R}^n$, where $\mathcal{Q}$ is the configuration space of the system with $n = 4$, x_b and y_b are the Cartesian coordinates of the base with respect to the treadmill origin, and δ_i is the translational position along the i^{th}-axis from the base position to the rod center of mass. Further, the continuous time state space has coordinates $x := (q^T, \dot{q}^T)^T \in \mathcal{X} \subseteq \mathbb{R}^8$. The control inputs $u \in \mathcal{U} \subseteq \mathbb{R}^2$ are two prismatic inputs for control on the base.

As in [31] we can begin our derivation of the dynamics with the rod center of mass as $p_p = p_b + L\mathbf{n}$, where $\mathbf{n}$ is a unit vector pointing from the base towards the pole mass center. We can then characterize the relative distance of the mass to the base as $L\mathbf{n} = (\delta_x, \delta_y, \delta_z)$, where L denotes the length from the base position to the center of mass, and δ_i is the translational position along the i^{th}-axis, with $\delta_z = \sqrt{L^2 - \delta_x^2 - \delta_y^2}$. We assume that the rigid pendulum is axi-symmetric, meaning that the principal moments of inertia of the pendulum about the rod length are identical and the pivot is located on the axis of symmetry. The Lagrangian can then be shown to be

$$\mathcal{L} = \frac{1}{2} m \dot{p}_p^T \dot{p}_p + \frac{1}{2} \Theta \Omega_{x,y}^T \Omega_{x,y} - m g^T p_p \qquad (2)$$
$$\Theta = \frac{1}{3} m L^2, \quad \Omega_{x,y} = \mathbf{n} \times \dot{\mathbf{n}}.$$

The nonlinear equations of motion can then be derived directly from the Lagrangian as

$$\frac{d}{dt}\left(\frac{\partial \mathcal{L}}{\partial \dot{x}}\right) - \frac{\partial \mathcal{L}}{\partial x} = Bu. \qquad (3)$$

where Bu is the vector of actuator forces. The kinetic energy is a quadratic, positive definite function of the generalized velocities, and so our resulting dynamics can be written in as the standard robotic equations [32]

$$D(q)\ddot{q} + H(q, \dot{q}) = Bu, \qquad (4)$$

where $D(q)$ is the inertia matrix, and $H(q, \dot{q}) = C(q, \dot{q}) + G(q)$ is the vector sum of the centrifugal, Coriolis, and the gravitational forces, respectively. For the pendulum, we would like to design a stabilizing controller u which can both balance the pendulum and drive it to a target position.

B. Control Methods and Integration on an Actuated Floor

We take a model based approach to pendulum control, using an infinite-horizon LQR controller on the linearized dynamics about the desired configuration of the pendulum on the treadmill, i.e. $q_0 = 0$, $\dot{q}_0 = 0$. The linearized dynamics are decoupled on the axes of the two inputs $u \in \mathbb{R}^m$, so we can instead consider a pair of identical controllers operating on their respective axes. For the x-direction, we can consider the linear system from the nonlinear dynamics (3) as

$$\begin{bmatrix} \dot{x}_b(t) \\ \dot{\delta}_x(t) \\ \ddot{x}_b(t) \\ \ddot{\delta}_x(t) \end{bmatrix} = \begin{bmatrix} 0 & 0 & 1 & 0 \\ 0 & 0 & 0 & 1 \\ \frac{3gm}{2L(m+4M)} & 0 & 0 & 0 \\ 0 & -\frac{3g(m+M)}{2L(m+4M)} & 0 & 0 \end{bmatrix} \begin{bmatrix} x_b(t) \\ \delta_x(t) \\ \dot{x}_b(t) \\ \dot{\delta}_x(t) \end{bmatrix} + \begin{bmatrix} 0 \\ 0 \\ \frac{4}{m+4M} \\ -\frac{3}{m+4M} \end{bmatrix} u(t), \quad t \geq 0, \quad x(0) = x_0 \qquad (5)$$

where the feedback control law $u(t) = -Kx(t)$ and $K \in \mathbb{R}^{n \times m}$, the control matrix, is designed such that the closed-loop system is asymptotically stable and the cost function

$$J(K) = \frac{1}{2} \int_0^\infty \left[x^T(t) Q x(t) + u^T(t) R u(t) \right] dt \qquad (6)$$

is minimized. The cost function can be tuned through the two matrices, Q and R, which are used to weight the system states and control inputs respectively. A simulation of the pendulum system is created and the weights Q and R are iteratively tuned to achieve the desired performance with desirable force responses to avoid saturation. These were then tuned on hardware to achieve the final performance. The control weights for the controller are given in Table I.

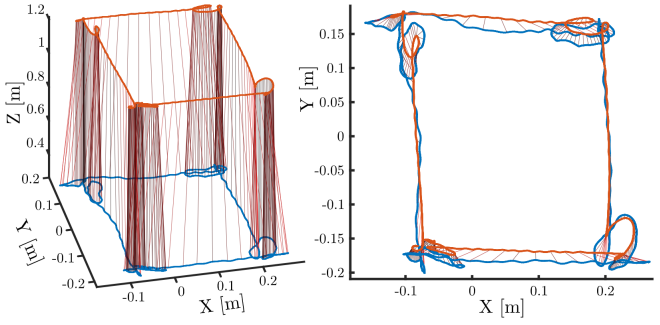

Fig. 4. Experimental results of the inverted pendulum dynamically tracking a square shape on the surface of the omnidirectional treadmill. Vertical lines are drawn at regular time intervals to represent the pendulum.

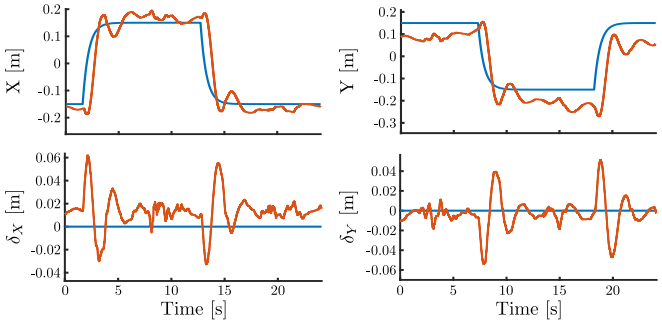

Fig. 5. Tracking performance on hardware for the pendulum when tasked with drawing a square shape. The top plots show global base positions while the bottom two show positions of the mass with respect to the base.

C. Experimental Results

In order to demonstrate the use of an actuated floor for balancing passive pendulums, we experimentally tested controllers for both stationary balancing and dynamic motion. The primary benchmark used to assess the controller was the tracking performance of a square. A 3D plot of the tracked square can be seen in Fig. 4, which visually illustrates the tracking during the experiment. The low level dynamics of the turning swashplates, as described in Section II, can be clearly seen as small sweeping motions when the controller needs the floor to change directions at corners. Despite these low-level disturbances to the commanded direction of the floor, the controller is able to stabilize the pendulum. In Fig. 5, the tracking error for both experiments can be seen. In the top plots we can see the pendulum base frame error while tracking a square traced on the floor, while in the bottom plots we can see the relative motion of the mass with respect to the base. When the tracking set point is changed, highly dynamic yet stable motion of the pendulum is achieved, as is shown by the large peaks in the bottom two plots.

IV. Passive Dynamic Walking With a Planar Biped

A passive dynamic walker is now introduced, which will be excited into passive dynamic walking along its frontal plane using control inputs only from an actuated environment. The developed controllers do not consider the sagittal plane, which we stabilize with the previously developed LQR controller (6). It will be shown that the designed orbits are stabilizing when applied as open loop velocity commands on the simulated system, and verified on hardware.

A. Passive Walker Model

A planar and passive bipedal armature was designed and constructed to test the ability of the actuated floor to induce passive dynamic walking, and is shown in Fig. 1. The armature was fabricated of aluminum framing to make it as rigid as possible to prevent spurious vibrational modes. The dimensions of the armature determined the practical achievable leg lift given our platform's acceleration. The stance width was largely chosen such that the walker would fit on the actuated surface and have enough room to ambulate. The armature has the ability to mount tuning weights if required, or passive appendages. Because the entire disk assembly on the floor is configured to drive all disk heads in a simultaneous parallel direction, the addition of rubber to the feet constrains the armature to be unable to turn left or right. The control approach we developed for this planar biped is decoupled to allow for a stable periodic orbit in the frontal plane and balance control in the sagittal plane. The

TABLE I
Control Parameters for the LQR Controllers

Control Parameters	m	L	Q	R
Pendulum	0.940	0.712	$[10, 75, 1, 1050]$	1.0
Passive Walker	6.956	0.788	$[5, 18, 1, 860]$	1.0

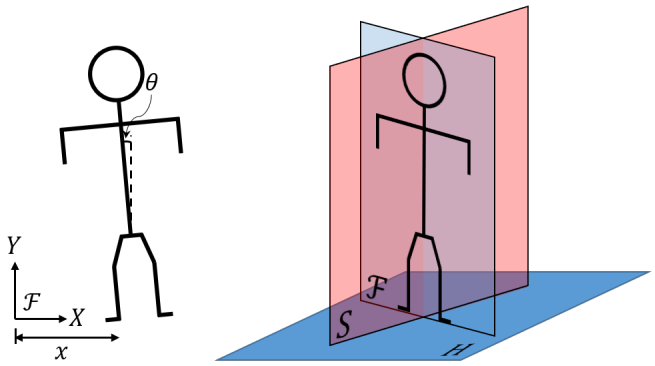

Fig. 6. Mathematical model of the planar walker showing: (a) the coordinate convention and (b) a depiction of the sagittal, frontal, and omnidirectional treadmill planes.

controller in the sagittal plane is identical to the controllers of the previously discussed pendulum, with the gains and model parameters as given in Table I. As such, we will develop a model for the 2D system projected to the frontal plane.

The coordinates of the planar biped in the frontal plane are the angle between the torso and the vertical axis, θ, and the horizontal position of the foot with respect to the global origin of the treadmill, x, as shown in Fig. 6. Then $q = (\theta, x) \in \mathbf{Q} \subset \mathbb{S}^1 \times \mathbb{R}$ is a set of generalized coordinates for the robot. As was the case for the inverted pendulum, we allow a single prismatic actuator at the floor to provide an input laterally, $u \in \mathcal{U} \subseteq \mathbb{R}^1$. In order to both keep the feet from freely moving during swing, and to induce a passive stabilizing effect on the orbit of the system, a very loose spring is added at the ankle. For the model used in simulation, we assume that the spring is 10 Nm/rad with a damping coefficient of 0.1 Nm/rad/s. This injects a very small amount of energy back into the system so that it can passively reject disturbances over several steps [33], but is loose enough that the robot will freely topple if it is not actively balanced. We can then follow the same Lagrangian approach to the dynamics as (3), with an additional term $\Gamma(q, \dot{q})$ due to the spring forces:

$$D(q)\ddot{q} + H(q, \dot{q}) = Bu + \Gamma(q, \dot{q}). \tag{7}$$

Having described the configuration of the passive walker, the set of equations obtained from (7) can also be expressed as the nonlinear affine control system [30]:

$$\dot{x} = f(x) + g(x)u, \quad \text{for} \quad x = (q^T, \dot{q}^T)^T. \tag{8}$$

The mathematical model of the hybrid system representation of locomotion we wish to design is defined based on the formal framework of hybrid systems. The (simple) hybrid system of the biped is defined as the tuple [9], [30]:

$$\mathscr{HC} = (\mathcal{D}, \mathcal{U}, S, \Delta, (f, g)) \tag{9}$$

- $\mathcal{D} \subseteq \mathbf{Q} \times \mathbb{R}^2$ is the *domain* consisting of admissible states on which (8) evolves,
- $\mathcal{U} \subseteq \mathbb{R}$ is the set of *admissible control inputs*,
- $S \subset \mathcal{D}$ is a guard (or switching surface) that are the states when the swing foot strikes the floor,

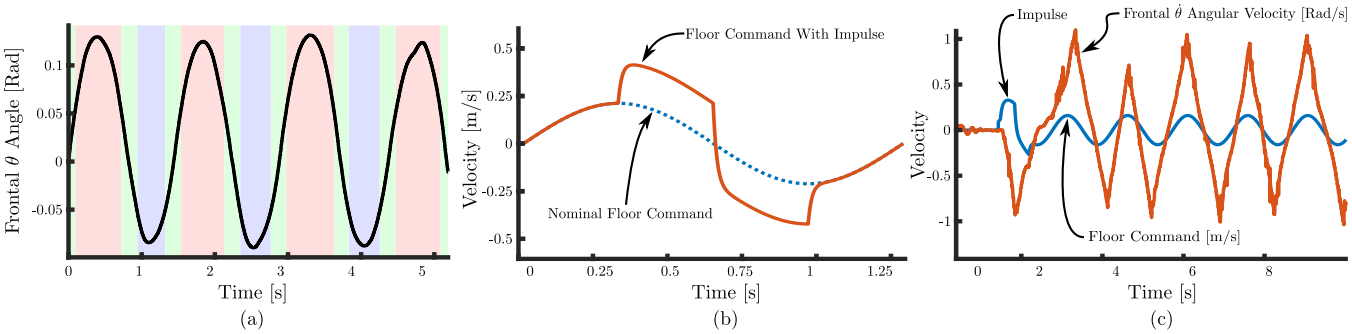

Fig. 7. (a) Experimental data for the torso angle of the passive dynamic walker on the frontal plane. Contact classification is shown as shaded sections, with green denoting a transition between double-support, red as right stance, and blue as left stance. (b) An example waveform of the impulse added to the open loop signal, which can excite locomotion from the neutral state. (c) Experimental data showing the robot excited into locomotion, and then falling into a periodic orbit. Pictured are the open loop treadmill velocity command, and the angular velocity $\dot{\theta}$ of the biped.

- $\Delta : S \subset \mathcal{D} \to \mathcal{D}$ is the *reset map* or *impact equations* that cause a discrete jump at impact,
- (f, g) is the *nonlinear control system* associated with the dynamics as given in (8).

Discrete dynamics determine the discrete change of robot states at impact. Given the pre-impact states $(q^-, \dot{q}^-) \cap S$, the post-impact states (q^+, q^+) are determined via the reset map Δ. Following the presentation in [11], the robot configuration is invariant through impact, i.e., $q^+ = q^-$. Due to the conservation of momentum, joint velocities will be subject to a discrete jump at impact, given by $\dot{q}^+ = \Delta_{\dot{q}}(\beta, q^-)\dot{q}^-$ where a coefficient of restitution for impact is given by $\beta \in [0, 1]$ which is 1 for a perfectly plastic impact. To model the impact as closely as possible to hardware, we use an estimated value of $\beta = 0.9$, so that our open loop trajectories better account for the loss of energy on hardware. Together, this defines the reset map Δ:

$$\begin{bmatrix} q^+ \\ \dot{q}^+ \end{bmatrix} = \Delta(\beta, q^-, \dot{q}^-) := \begin{bmatrix} \Delta_q(q^-) \\ \Delta_{\dot{q}}(\beta, q^-)\dot{q}^- \end{bmatrix}. \tag{10}$$

Because we are only concerned with designing period one orbits for symmetric walking, we can model $\Delta_q(q^-) := \mathcal{R}q^-$ where $\mathcal{R}$ is a relabeling matrix which mirrors the configuration of the robot to the other leg. Given these definitions for the passive dynamic model, we formulate an optimization from which we can drive the robot into a periodic walking cycle. This will be ultimately started from a standing position, so that the system can be autonomous with the exception of a user dictating the start of the walking.

When the robot is resting flat on the ground, it is only unstable in the sagittal plane, and can be treated as an inverted pendulum in that direction. In this configuration we define a neutral position, which is a minimal energy state of the robot and manifests itself as a fixed point in the phase space of the system. This can be seen at the center of the limit cycle shown in Fig. 9, where the robot begins it's motion. By injecting energy along the frontal plane, we can then induce a periodic orbit for passive dynamic locomotion.

B. Control for Passive Dynamic Walking

A straightforward and intuitive approach to formulate an optimization for a simple periodic orbit such as this is via direct single shooting methods. In this, we simulate the solution $\phi_\alpha(x_0, t)$ of the hybrid system $\mathscr{HC}$ with initial condition x_0 via a single time-marching numerical integration of the system dynamics subject to the feedback controller: $u_\alpha(x(t), t)$ dependent on control parameters α. In order to verify the existence and stability of periodic orbits, the method of Poincaré sections was used with the guard S defined for the hybrid system in (9) serving as the Poincaré section, as in [30], [34]. Let the time-to-impact function $T_I : S \to \mathbb{R}$ represent the time from initialization (on the guard) to the first intersection with S. Then, the Poincaré return map $P : S \to S$ which represents the new state of the figure after one step becomes:

$$P_\alpha(x(t)) = \phi_\alpha(T_I \circ \Delta(x(t)), \Delta(x(t))). \tag{11}$$

An optimization problem yields the control parameters:

$$\begin{aligned} \alpha^* = \underset{\alpha}{\text{argmin}} & \int_0^T ||u_\alpha(x(t), t)||^2 dt \\ \text{s.t.} \quad & \dot{x}(t) = f(x(t)) + g(x(t))u_\alpha(x(t), t) \\ & P_\alpha(x(T)) - x(T) = 0 \end{aligned} \tag{12}$$

where T is a specified step duration for the trajectory, and the constraint on the Poincaré map enforces periodicity.

In the following discussion, two control inputs will be considered: $u_{\alpha^*}(x(t), t)$, the optimized closed loop control input (from (12)), and $\hat{u}(t)$, a least squares sinusoidal parameterization of $u_{\alpha^*}(x(t), t)$. The resulting open loop floor acceleration waveform $\hat{u}$ was used as the control input for the physical system, and can be seen in Fig. 7 (c). The stability of the orbit generated by the open loop trajectory was confirmed in simulation with the Poincaré map by ensuring that the magnitude of the maximum eigenvalue was less than 1. Because the initial configuration of the biped is at the fixed point (corresponding to standing upright), a large perturbation is required to enter the limit cycle induced by $\hat{u}$. In order to achieve this, an initial high acceleration disturbance of the form of two consecutive opposite signed square waves was designed to induce the passive dynamic side-to-side walking behavior, as seen in Fig. 7. (b).

The controller which was introduced for balancing in the forward direction (6) requires accurate knowledge of

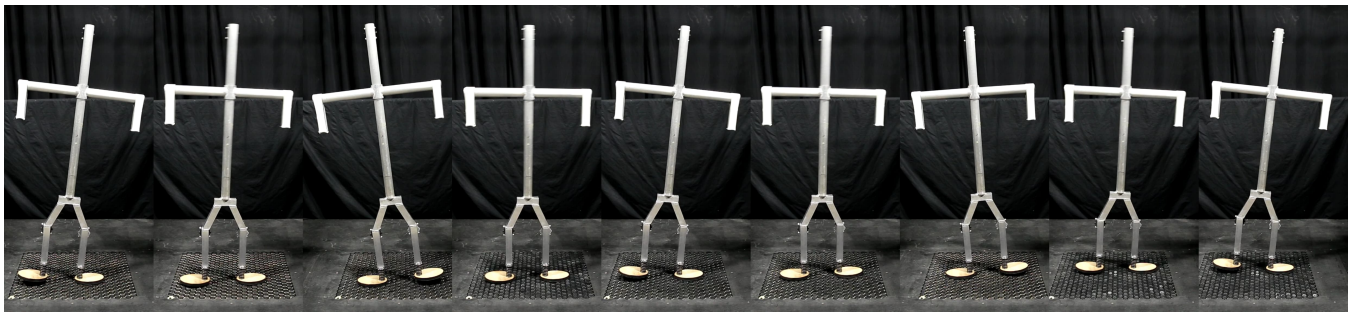

Fig. 8. Tiles showing the passive biped walking with an actuated floor. The periodic nature of the passive dynamics excited by the floor can be seen.

the current contact point on the ground to keep the robot upright. As such, we implemented a smooth contact detection scheme which was based on implementations previously used on actuated bipedal robots [35]. For this, we utilize the mathematical concept of fuzzy sets, so as to have a gradual shift of the pendulum base position between the stance feet while transitioning load, when the uncertainty of the contact is highest. We can define the current stance phase of a leg by the fuzzy set $A = \{(\theta, \mu_{st}(\theta))|\mu_{\text{st}}(\theta) \mapsto [0,1]\}$ where the membership function $\mu(\theta)$ is given by

$$\mu_{\text{st}}(\theta) = \begin{cases} 0 & \theta < \bar{\theta}_{\text{lf}} \\ \frac{\theta - \bar{\theta}_{\text{lf}}}{\bar{\theta}_{\text{rf}} - \bar{\theta}_{\text{lf}}} & \bar{\theta}_{\text{rf}} \leq \theta \leq \bar{\theta}_{\text{lf}} \\ 1 & \bar{\theta}_{\text{rf}} \end{cases}, \tag{13}$$

and the values for $\bar{\theta}_{\text{rf}}$, $\bar{\theta}_{\text{lf}}$ are the fuzzy upper and lower limits. We then simply say that if $\mu(\theta) = 1$ that we are confident that the right leg is stance, and if $\mu(\theta) = 0$ that left is stance. The position of the base can then be used in the LQR controller as

$$x_b = \mu(\theta) \cdot x_{\text{rf}} + (1 - \mu(\theta)) \cdot x_{\text{lf}}. \tag{14}$$

In Fig. 7 (a), we visually demonstrate this on experimental data. In green regions $\mu(\theta)$ is transitioning support, whereas red and green denote $\mu(\theta) = 0$ and $\mu(\theta) = 1$, respectively.

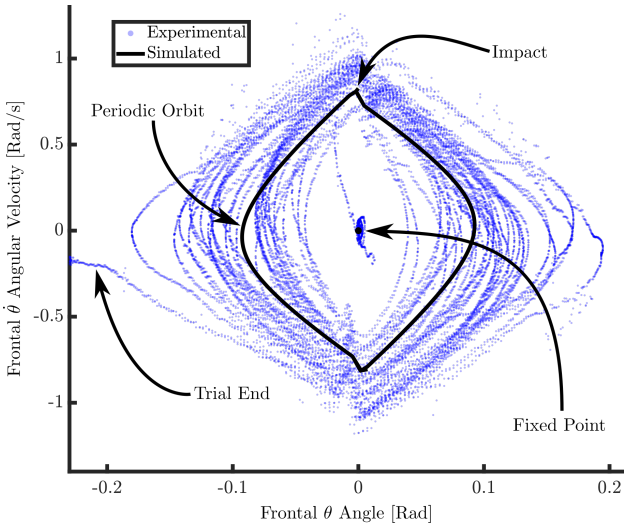

Fig. 9. Stable periodic orbit achieved by the planar walker experimentally. The evolving periodic orbit is shown along with the initial condition of the system at the fixed point, and convergence to the orbit from this fixed point.

C. Experimental Results

Passive dynamic walking was verified both in simulation and experimentally on the passive dynamic walker. In Fig. 7 (c), the open loop velocity command obtained from the optimization (12) is shown as commanded on hardware. The phase matched angular velocity response of the biped to the excitation of the floor can also be seen. A time sequence over two steps of walking is pictured in Fig. 8. The walking pictured was started from the neutral configuration, and excited via a square wave pictured in Fig. 7 (b). This can be seen clearly as a large amplitude spike in Fig. 7 (c), after which the system falls into a stable periodic orbit. This orbit is shown in Fig. 9, along with convergence to the orbit starting from rest, i.e., starting from the fixed point shown in Fig. 9 the walker converges to the periodic orbit. This, therefore, experimentally demonstrates the existence of stable passive dynamic locomotion with an actuated floor.

V. Conclusions and Future Work

This paper has shown the ability to demonstrate passive dynamic walking experimentally through the use of actuated environments. Using actuated environments to enable or assist in balance and locomotion for simple semi-anthropomorphic structures can simplify the design of balancing robots. The use of the external mechanism eliminates or reduces the constraints and tradeoffs inherent in designing a fully independent robot. Of course, these simplified robots must live on platforms with high agility (such as the novel omnidirectional treadmill used in this work), but their study can give insight into the mechanisms underlying dynamic locomotion. Although the robots considered here are completely passive, this method can be extended to robots that have the actuation necessary to perform more expressive movements, but do not have the actuation required to balance themselves. Finally, we envision robots that share the balancing load between internal actuation and these external actuated environments.

Acknowledgment

The authors would like to thank Elizabeth Alderman for her previous work on the actuated floor and the members of Disney Research for their helpful discussions and support.

REFERENCES

[1] Tad McGeer et al. Passive dynamic walking. *I. J. Robotic Res.*, 9(2):62–82, 1990.

[2] Ambarish Goswami, Bernard Espiau, and Ahmed Keramane. Limit cycles and their stability in a passive bipedal gait. In *Proceedings of IEEE International Conference on Robotics and Automation*, volume 1, pages 246–251. IEEE, 1996.

[3] Arthur D Kuo. Stabilization of lateral motion in passive dynamic walking. *The International journal of robotics research*, 18(9):917–930, 1999.

[4] Steven H Collins, Martijn Wisse, and Andy Ruina. A three-dimensional passive-dynamic walking robot with two legs and knees. *The International Journal of Robotics Research*, 20(7):607–615, 2001.

[5] Steve Collins, Andy Ruina, Russ Tedrake, and Martijn Wisse. Efficient bipedal robots based on passive-dynamic walkers. *Science*, 307(5712):1082–1085, 2005.

[6] Mark W Spong and Francesco Bullo. Controlled symmetries and passive walking. *IEEE Transactions on Automatic Control*, 50(7):1025–1031, 2005.

[7] Ryan W Sinnet and Aaron D Ames. Energy shaping of hybrid systems via control lyapunov functions. In *2015 American Control Conference (ACC)*, pages 5992–5997. IEEE, 2015.

[8] Martijn Wisse, Guillaume Keliksdal, Jan Van Frankenhyyzen, and Brian Moyer. Passive-based walking robot. *IEEE Robotics & Automation Magazine*, 14(2):52–62, 2007.

[9] Aaron D Ames, Robert D Gregg, and Mark W Spong. A geometric approach to three-dimensional hipped bipedal robotic walking. In *2007 46th IEEE Conference on Decision and Control*. IEEE, 2007.

[10] Marc H Raibert. *Legged robots that balance*. MIT press, 1986.

[11] Eric R Westervelt, Jessy W Grizzle, Christine Chevallereau, Jun-Ho Choi, and Benjamin Morris. *Feedback Control of Dynamic Bipedal Robot Locomotion*. Taylor & Francis/CRC, 2007.

[12] Jenna Reher, Eric A Couisineau, Ayonga Hereid, Christian M Hubicki, and Aaron D Ames. Realizing dynamic and efficient bipedal locomotionon the humanoid robot DURUS. *IEEE International Conference on Robotics and Automation (ICRA)*, pages 1794–1801, 2016.

[13] Brian G Buss, Alireza Ramezani, Kaveh Akbari Hamed, Brent A Griffin, Kevin S Galloway, and Jessy W Grizzle. Preliminary walking experiments with underactuated 3D bipedal robot MARLO. *IEEE/RSJ International Conference on Intelligent Robots and Systems*, pages 2529–2536, 2014.

[14] Jenna Reher, Wen-Loong Ma, and Aaron D Ames. Dynamic walking with compliance on a Cassie bipedal robot. In *2019 18th European Control Conference (ECC)*, pages 2589–2595. IEEE, 2019.

[15] W. Bosworth, S. Kim, and N. Hogan. The MIT super mini cheetah: A small, low-cost quadrupedal robot for dynamic locomotion. In *2015 IEEE International Symposium on Safety, Security, and Rescue Robotics (SSRR)*, pages 1–8, Oct 2015.

[16] Huihua Zhao, Eric Ambrose, and Aaron D Ames. Preliminary results on energy efficient 3D prosthetic walking with a powered compliant transfemoral prosthesis. In *2017 IEEE International Conference on Robotics and Automation (ICRA)*, pages 1140–1147. IEEE, 2017.

[17] Steven H Collins, M Bruce Wiggin, and Gregory S Sawicki. Reducing the energy cost of human walking using an unpowered exoskeleton. *Nature*, 522(7555):212, 2015.

[18] Tony Dear, Scott David Kelly, and Howie Choset. Variations on the role of principal connections in robotic locomotion. In *ASME 2016 Dynamic Systems and Control Conference*. American Society of Mechanical Engineers Digital Collection, 2016.

[19] Robert Bristow, David Loyal Christensen, Günter D Niemeyer, and Lanny S Smoot. Floor system providing omnidirectional movement of a person walking in a virtual reality environment, September 17 2019. US Patent 10,416,754.

[20] Lanny S Smoot and Cynthia Rueyi Sung. System for providing multi-directional and multi-person walking in virtual reality environments, March 12 2019. US Patent 10,228,758.

[21] David Loyal Christensen, Günter D Niemeyer, and Lanny S Smoot. System for stabilizing an object to control tipping during omnidirectional movement, September 19 2018. US Patent Application.

[22] Shozo Mori, Hiroyoshi Nishihara, and Katsuhisa Furuta. Control of unstable mechanical system control of pendulum. *International Journal of Control*, 23(5):673–692, 1976.

[23] Rong Yang, Yiu-Yiu Kuen, and Zexiang Li. Stabilization of a 2-DOF spherical pendulum on xy table. In *Proceedings of the 2000. IEEE International Conference on Control Applications. Conference Proceedings (Cat. No. 00CH37162)*, pages 724–729. IEEE, 2000.

[24] Jinglai Shen, Amit K Sanyal, Nalin A Chaturvedi, Dennis Bernstein, and Harris McClamroch. Dynamics and control of a 3D pendulum. In *2004 43rd IEEE Conference on Decision and Control (CDC)(IEEE Cat. No. 04CH37601)*, volume 1, pages 323–328. IEEE, 2004.

[25] Nalin A Chaturvedi, Taeyoung Lee, Melvin Leok, and N Harris McClamroch. Nonlinear dynamics of the 3D pendulum. *Journal of Nonlinear Science*, 21(1):3–32, 2011.

[26] Olfa Boubaker. The inverted pendulum: A fundamental benchmark in control theory and robotics. In *International conference on education and e-learning innovations*, pages 1–6. IEEE, 2012.

[27] Shuuji Kajita, Fumio Kanehiro, Kenji Kaneko, Kazuhito Yokoi, and Hirohisa Hirukawa. The 3D linear inverted pendulum mode: A simple modeling for a biped walking pattern generation. In *Proceedings 2001 IEEE/RSJ International Conference on Intelligent Robots and Systems. Expanding the Societal Role of Robotics in the the Next Millennium (Cat. No. 01CH37180)*, volume 1, pages 239–246. IEEE, 2001.

[28] Miomir Vukobratović and Branislav Borovac. Zero-moment point-thirty five years of its life. *International journal of humanoid robotics*, 1(01):157–173, 2004.

[29] Jerry Pratt, John Carff, Sergey Drakunov, and Ambarish Goswami. Capture point: A step toward humanoid push recovery. In *2006 6th IEEE-RAS international conference on humanoid robots*, pages 200–207. IEEE, 2006.

[30] Jessy W Grizzle, Christine Chevallereau, Ryan W Sinnet, and Aaron D Ames. Models, feedback control, and open problems of 3D bipedal robotic walking. *Automatica*, 50(8):1955–1988, 2014.

[31] Dario Brescianini, Markus Hehn, and Raffaello D'Andrea. Quadrocopter pole acrobatics. In *2013 IEEE/RSJ International Conference on Intelligent Robots and Systems*, pages 3472–3479. IEEE, 2013.

[32] Richard M. Murray, Zexiang Li, Sastry, and S. Shankar Sastry. *A mathematical introduction to robotic manipulation*. CRC press, 1994.

[33] Michael Ernst, Hartmut Geyer, and Reinhard Blickhan. Extension and customization of self-stability control in compliant legged systems. *Bioinspiration & biomimetics*, 7(4):046002, 2012.

[34] Eric Wendel and Aaron Ames. Rank properties of Poincaré maps for hybrid systems with applications to bipedal walking. In *HSCC'10 - Proceedings of the 13th ACM International Conference on Hybrid Systems: Computation and Control*, pages 151–160, 01 2010.

[35] Siavash Rezazadeh, Christian Hubicki, Mikhail Jones, Andrew Peekema, Johnathan Van Why, Andy Abate, and Jonathan Hurst. Spring-mass walking with Atrias in 3D: Robust gait control spanning zero to 4.3 kph on a heavily underactuated bipedal robot. In *ASME 2015 dynamic systems and control conference*. American Society of Mechanical Engineers Digital Collection, 2016.